Int. J. Mach. Learn. & Cyber. (2013) 4:85–98
DOI 10.1007/s13042-012-0076-x

ORIGINAL ARTICLE

# Modeling, simulation and design optimization of a hoisting rig active heave compensation system

**Peter Gu · Ahmed Ahmed Walid · Yousef Iskandarani · Hamid Reza Karimi**

Received: 10 September 2011 / Accepted: 21 January 2012 / Published online: 3 February 2012


**Abstract** The objective of this paper is to present an approach in developing a virtual active heave compensation system for a draw-works on a hoisting rig. A virtual system enables quicker overall product development time of a physical system as well as flexibility in optimizing the design parameters. Development of the virtual system started with the modelling of the draw-works and hoisting rig dynamics. Simulations of this model were run in two operational modes while subject to a sinusoidal wave: heave compensation and seabed landing of a payload. The results were analyzed and used for optimization in terms of cost and performance. This lays the groundwork for further testing either through hardware-in-the-loop testing (HIL) or using an actual prototype.

**Keywords** Active heave compensation (AHC) · Draw-works · Hoisting rig · Modeling · Simulation

## 1 Introduction

The operation of hoisting machinery out at sea poses the problem of wave induced heave motion interfering with the positioning of a payload. This problem exists in six degrees of motion, but heave motion is the most problematic. Motion interference also causes great variations in the forces transferred through the hoisting wire and further onto the mechanical hoisting system itself which may cause structural damage. Four main scenarios of payload hoisting operations at sea are affected by heave motion: (1) above water, (2) water entry, (3) submerged, but not in contact with the seabed, (4) lowering onto the seabed. Thus, without systems that compensate for heave motion, hoisting operations at sea face frequent downtime risks.

Over the years, passive, active and semi-active heave compensation systems have been researched and developed in order to lessen the problems associated with heave motion interference [1–7]. Passive heave compensation (PHC) systems such as drill string compensators and riser tensioners have been in use since the 1970s and are still in widespread use. They function essentially as springs to absorb the forces generated as a rig heaves in relation to a payload while it is in contact with the seabed, in other words during contact operation. Current compensators are able to carry up to $\sim$450,000 kg payloads with load variation less than 5% during contact operation [8]. Recent research on PHC systems include the work by Driscoll et al. [9] who found stiffness and damping characteristics of a passive cage-mounted heave compensator. Another work on PHC is by J. Ni et al. [10] who proposed a PHC system with accumulators.

PHC systems are less costly compared with AHC systems and perform well during contact-operations, however their performance during non-contact operations have larger limitations. According to a document by the Integrated Ocean Drilling Program–United States Implementing Organization (IODP–USIO) PHC systems have ca. 85% efficiency in heave compensation when ship heave is $> \sim$4 m, but only ca. 40% when ship heave is $< \sim$2 m [11]. The large variation in heave compensation efficiency for different ship heave conditions is one of PHC systems' weaknesses.

On the other hand, AHC systems are able to vary the compensation according to the actual conditions and are therefore more accurate with heave compensation

P. Gu · A. A. Walid · Y. Iskandarani · H. R. Karimi (✉)
Department of Engineering, Faculty of Engineering and Science, University of Agder, 4898 Grimstad, Norway
e-mail: hamidrk@uia.no

efficiencies of ca. 95% in any ship heave condition [11]. Recent work on AHC systems include Neupert et al. [12] who presented a combination of trajectory tracking disturbance decoupling controller and a prediction algorithm for an AHC system. Li and Liu in Ref. [13] proposed three-degree-of-freedom dynamic models of an AHC system subject to a sinusoidal wave. Furthermore, in order to strengthen the safety and to monitor the working states of numerical control system real time, a framework was developed in [14] to diagnose multi-kinds of potential connection-related faults in the system.

This paper details the development of a virtual AHC system for a hoisting rig. By modeling and simulating such a system design optimization in terms of cost and performance can be achieved before actual prototype production. This is done for the entire system which includes the hydraulic, mechanical and control components. The entire process is threefold: system modeling and simulation, cost and performance optimization, and finally testing using hardware-in-the-loop (HIL) methodology. The result is a more time and cost efficient product development procedure. This paper covers the process of modeling, simulation and design optimization of the AHC system. It does not include the HIL testing which constitutes future work. Zheng et al. [15] proposed HIL testing with both mathematical models and physical components of an AHC system on a pipeline lifting mining system.

On the other hand, economic production in an imperfect production system; i.e. a system in which the machine shifts from an 'in-control' state to an 'out-of-control' state, has been broadly investigated in the literature, see for instance [16]. Therefore, for an AHC system, cost optimization is included to illustrate the financial side of designing such a system. Dimensionless cost units are assigned to the components used in the design. They give a rough suggestion as to the value of each component, but do not represent real world costs of the components. By including the results of the cost optimization the authors hope to show how this facet of product development influences the rest of the design process. Again, this by no means represents real world costs, but is only for illustration. Recently, in Ref. [17], a robust self-learning proportional–integral–derivative control system design is developed for non-linear systems based on a particle swarm optimization algorithm.

Similar work (without cost optimization) has recently been done by Zhang et al. [18], where a semi-active heave compensation system for a deep sea poly-metallic mining system was developed. The model and subsequent simulation were done to ensure necessary design performance and robustness requirements were met.

## 2 Problem formulation

The problem at hand is the performance and cost optimization of a virtual AHC system applied on a hoisting rig. As fundamental requirements such a system, it should handle two load cases with a submerged payload while under the influence of a heave motion: (1) position stabilization along a vertical axis and (2) lowering of 5 m to the seabed. Heave compensation must decrease the oscillations of the payload by at least 95%, which is the present competitive efficiency for such a system. This reduces excessive loads transferred to the wire and the rest of the hoisting machinery. The lowering time should be less than 10 s and a seabed landing with no significant impact loads should be achieved. The AHC model is to be run for load case 1 and 2 under the influence of a constant sinusoidal heave motion. The payload must land smoothly on the seabed to avoid large impact loads. The cost and performance of the system must be optimized based on the simulation results. There is no consideration for fracture or fatigue of the mechanical system. This is not the aim of the project, so as long as the steady state forces are within the design limits the design is considered satisfactory.

Modeling of the AHC system requires three main parts: the mechanical, hydraulic and control system. The mechanical system consists of components of the hoisting rig that are important to the overall dynamics. This includes the drums, sheaves, wire, travelling block, payload and the rig itself. The hydraulic part consists of the hydraulic circuit that actuates the mechanical system. This is also where the control elements are located: the servo valves and displacement pump. The control system regulates the hydro-mechanical system through the control elements using a controller algorithm.

## 3 Mechanical system modeling

The modeling and simulation of the mechanical system is based on the minimum sheave configuration of three sheaves. This minimum number is based on the assumption that having no gearing from the sheave system will yield too high of a cost on the hydraulic side. The three sheaved configuration is not necessarily the most efficient arrangement in terms of cost or performance, but its modeling process is shown in this paper due to its simplicity. Modeling and simulation of sheave configurations with more sheaves follow the same principle as that of the three sheaves system. In the end the most cost efficient design will be used and simulated. The overall mechanical system is illustrated in Fig. 1.

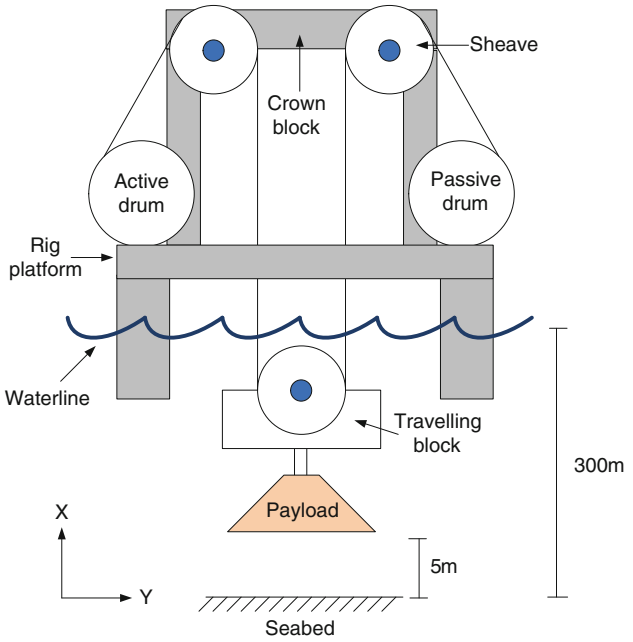


**Fig. 1** Hoisting rig schematic

### 3.1 Static analysis and dimensioning

A static force analysis was performed to get a quick overview of the basic dimensions of the hoisting rig. The starting point was a mechanical concept with three sheaves in total. Although the finally chosen concept consisted of seven sheaves in total, the modeling process was the same in principle. Data for wire force and active drum torque were found which were used to dimension a selection of design parameters. Table 1 shows these parameters among others.

The method of analysis is to draw free body diagrams (FBD's) for each component starting with the payload and ending with the active drum. Equilibrium equations are subsequently set up isolating the unknown variable. The actual static calculations are not included as this is not the focus of this paper. However, the results are included in Table 1. They constitute the initial dimensions of the system and are used in the dynamic analysis and subsequent simulation.

The end disk diameter $d_{DE}$ of the active drum was dimensioned with the capability of storing 300 m of wire, but in reality only a fraction of this is needed. This is because the active drum only operates during the active phase, in other words load case 1 and 2. The active drum dimensions are illustrated in Fig. 2.

Considerations taken in the static analysis:

- Buoyancy of payload.
- Weight of payload and travelling block.

Simplifications in the static analysis:

**Table 1** Initial parameters for the three-sheaved mechanical system

| Component | Parameter | Symbol | Quantity |
|---|---|---|---|
| Payload | Mass | $m_{pl}$ | 10,000 kg |
| | Cross sectional area | $A_{pl}$ | 1.5 $m^2$ |
| Travelling block | Mass | $m_{tb}$ | 400 kg |
| | Cost | $C_{tb}$ | 1.65 |
| Wire | Inner section mass | $m_i$ | 525 kg |
| | Outer section mass | $m_o$ | 87.5 kg |
| | Volume per wire section | $V_w$ | 0.06 $m^3$ |
| | Force | W | 40,940 N |
| | Diameter | $D_w$ | 22 mm |
| | Nr. of wire sections from crown to travelling block | $N_w$ | 2 |
| | Cost | $C_w$ | 0.79 |
| Sheave | Mass | $m_{sh}$ | 26 kg |
| | Inner diameter | $D_{sh\_i}$ | 75 mm |
| | Outer diameter | $D_{sh}$ | 525 mm |
| | Cost | $C_{sh}$ | 0.47 |
| Active drum | Torque | $\tau_{drum}$ | 12,880 Nm |
| | Diameter | $D_{drum}$ | 440 mm |
| | Width | $B_d$ | 440 mm |
| | Thickness | $h_D$ | 320 mm |
| | End disk diameter | $d_{DE}$ | 710 mm |
| | Cost | $C_{ad}$ | 1.45 |

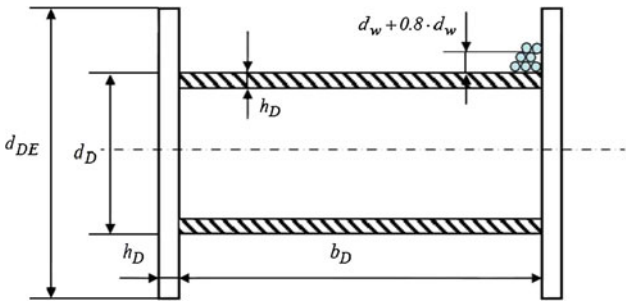


**Fig. 2** Active drum dimensions

- No friction between sheave bearing and sheave.
- Wire considered as massless non elastic rods. Wire weight effect was instead estimated using a factor multiplied with the wire force.
- No dynamics involved; the system is in equilibrium.
- Wire rope wear is assumed to be non-problematic.

An adverse effect that the static analysis does not take into account is wire wear due to bending of the wire as it goes through a sheave. This effect is more pronounced with an AHC system because of the constant adjusting of wire to keep wire tension and payload position at desirable levels. To account for this adverse effect the ratio between wire

and sheave diameter $D_{sh}/D_w$, also known as strength efficiency [19], must be considered. In this case the ratio of $\sim$24 is assumed to be enough.

### 3.2 Linear dynamics analysis

Equations of motion are set up for the mechanical system. In these equations the dimensions found in the static analysis are to be used initially. Necessary changes will be done after simulations have been run for the model. The simulation software *SimulationX* by *ITI GmbH* was used.

The actual modeling follows the same strategy as in the static analysis. Free body diagrams and kinetic diagrams (KD's) are drawn from the payload and upwards to the active drum. The dynamic analysis takes into account:

- Friction between sheave bearing pin and sheave.
- Slippage between wire and sheave.
- Inertia of sheaves, drum, combined payload and wire.
- Wire dynamics: stiffness, damping, elongation and rate of elongation.
- Wire weight.
- Wire buoyancy.
- Seabed dynamics.
- Hydrodynamic drag.

#### 3.2.1 Simplifications

Simplifications include having a constant active drum and wire mass. This is justified by the limited movement that the system goes through in load case 1 and 2. The passive drum is not in operation during the load cases, thus it is neglected and the wire to it is seen as anchored to the rig platform.

The wire mass is divided into upper and lower sections. The lower wire section mass of wire 1 and 2 have been combined with the mass of the payload, sheave 2 and travelling block. This method also allows the effect of wire elongation due to wire mass to be approximated.

Internal friction in the wire can be significant due to its bending as it goes through a sheave. However, this varies according to the type and configuration of sheave and wire. For simplification, it is assumed that this internal friction is insignificant.

The overall hoisting rig dynamic model schematic can be seen in Fig. 3.

#### 3.2.2 Combined payload

The geometry of the combined payload is assumed to be such that only an insignificant amount of sea water is trapped, therefore this entrained water mass is not included Fig. 4. The equivalent equation for the FBD and KD is:

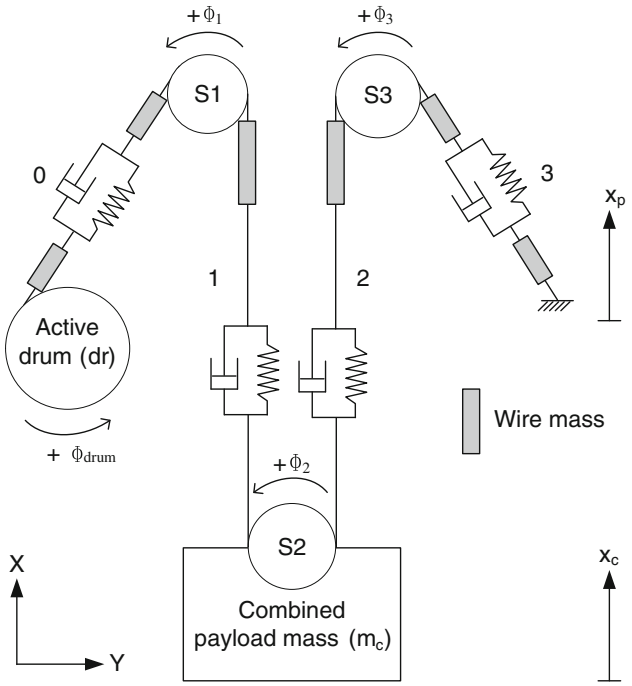


**Fig. 3** Hoisting rig dynamic model schematic

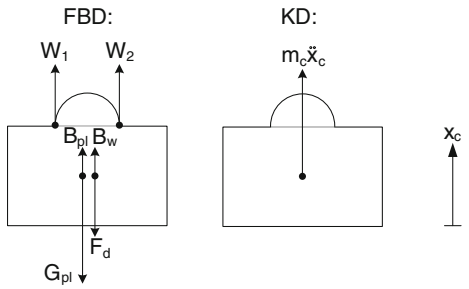


**Fig. 4** The FBD and KD of the combined payload

$$W_1 + W_2(\dot{x}_c)\, F_d + B_w + B_{pl} - m_c g + F^*_{sb} = m_c \ddot{x}_c \qquad (1)$$

where the combined payload mass is $m_c = m_{pl} + m_{tb} + m_{sh} + \frac{1}{2} n_w m_i$ and the wire and payload buoyancy are $B_w = V_w g$ and $B_{pl} = V_{pl}\, g$ respectively. The drag force is $F_d = \frac{1}{2} \rho A_{pl} C_d \dot{x}_c$, where the water density is $\rho = 1027 \frac{kg}{m^3}$ and the drag coefficient is assumed to be $C_d = 1,8$.

A seabed interaction force is commonly modeled by a spring and damper pair or simply a spring, since the spring effect will usually dominate the damping effect [13]. Thus, the seabed force $F_{sb}$ is modeled as a spring-damper as shown in Fig. 5. It is only in effect when the payload position $x$ is below the seabed level. This gives $F_{sb} = k_{sb} \times x + c_{sb} \times \dot{x}$, where spring coefficient is $k_{sb} = 10^6 \frac{N}{m}$ and damping coefficient is $c_{sb} = 10^2 \frac{Ns}{m}$. $^*F_{sb}$ only acts when the payload is in contact with the seabed.

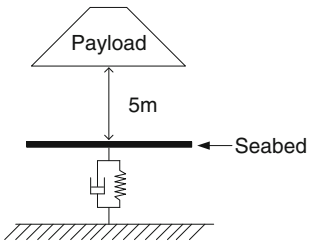


**Fig. 5** Seabed dynamics

*Remark 1* It is worth noting that there has been a significant attention to develop time-domain models for simulation and control system design based on data obtained from seakeeping programs such as VERES [20] and WAMIT [21]. These programs are used to compute the potential coefficients for a vibratory spring-damper model and the existing wave loads (Froude–Krylov and diffraction forces) for a given vessel design (see for instance [22–24] and the references therein).

### 3.2.3 Wire force

The wire can be regarded as an elastic rod and therefore modeled as a spring. Damping is also added to this model to account for internal friction in the wire. Therefore, the general wire force equation is $W = F_s + F_d$, where the spring force is derived from Hooke's law: $F_s = k\delta$. The damper force is $F_d = c\dot{\delta}$. The damper coefficient $c$ is defined as 10% of the spring coefficient. However, this is only a rough estimate and may not reflect the actual value. This gives the following for the wire forces:

$$W_0 = k_o\delta_0 + c_o\delta_0 \tag{2}$$

$$W_1 = k_i\delta_1 + c_i\delta_1 \tag{3}$$

$$W_2 = k_i\delta_2 + c_i\delta_2 \tag{4}$$

$$W_3 = k_o\delta_3 + c_o\delta_3 \tag{5}$$

### 3.2.4 Wire elongation

The wire elongation in each wire section is determined by the difference in rotational displacement by the sheaves. In addition to this, it is known by the difference between the heave motion $z(t)$ and the motion of the combined payload $x(t)$. The passive drum is not in the scope of this project and thus does not affect the wire elongation. This gives the following equations:

$$\delta_0 = \phi_{drum}\frac{D_{drum}}{2} - \phi_1 r_1 \tag{6}$$

$$\delta_1 = \phi_1 r_1 + z(t) + \phi_2 r_2 - x(t) \tag{7}$$

$$\delta_2 = -\phi_2 r_2 + z(t) - \phi_3 r_3 - x(t) \tag{8}$$

$$\delta_3 = \phi_3 r_3 \tag{9}$$

which are valid for $\delta_n \geq 0$, but 0 for $\delta_n < 0$. This is because no wire compression (negative elongation) is modeled. The wires are thought to be slacking by that time. The heave motion $z(t)$ consists of a sine wave with 1 m in amplitude and frequency of 0.1 Hz:

$$z(t) = \sin(2 \times \pi \times f \times t) \tag{10}$$

### 3.2.5 Wire rate

Wire rate in each wire section is described by the following equations:

$$\dot{\delta}_0 = \dot{\phi}_{drum}\frac{D_{drum}}{2} - \dot{\phi}_1 r_1 \tag{11}$$

$$\dot{\delta}_1 = \dot{\phi}_1 r_1 + \dot{z}(t) + \dot{\phi}_2 r_2 - \dot{x}(t) \tag{12}$$

$$\dot{\delta}_2 = -\dot{\phi}_2 r_2 + \dot{z}(t) - \dot{\phi}_3 r_3 - \dot{x}(t) \tag{13}$$

$$\dot{\delta}_3 = \dot{\phi}_3 r_3 \tag{14}$$

### 3.2.6 Wire weight

The inner wires of the lower wire sections are seen as part of the combined payload mass, thereby having its mass and inertia modeled as part of this component. The other wire mass sections are modeled on their own, see Fig. 6.

The equivalent equations for the FBD's are:

$$W_{1u} - \frac{W_{mi}}{2} - W_1 = 0 \tag{15}$$

$$W_{2u} - \frac{W_{mi}}{2} - W_2 = 0 \tag{16}$$

$$W_{0u} - \frac{W_{mo}}{2} - W_0 = 0 \tag{17}$$

$$W_{3u} - \frac{W_{mo}}{2} - W_3 = 0 \tag{18}$$

$$W_0 - \frac{W_{mo}}{2} - W_{1l} = 0 \tag{19}$$

$$W_3 - \frac{W_{mo}}{2} - W_{2l} = 0 \tag{20}$$

where $W_{mi} = m_i \times g$ and $W_{mi} = m_o \times g$ .

### 3.2.7 Sheaves

The upper sheaves are fixed to the crown block of the drilling rig. This means they have no acceleration in relation to the overall system. Hence, no kinetic diagram is drawn for these sheaves. The FBD's of the crown block sheaves are shown in Fig. 7.

The equivalent equations for the FBD's are:

$$N_1 - G_{sh} - W_{1l} - W_{1l} = 0 \tag{21}$$

$$N_3 - G_{sh} - W_{2u} - W_{3u} = 0 \tag{22}$$

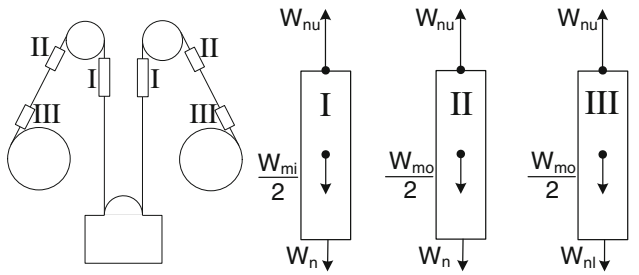


**Fig. 6** FBD's of the upper inner (*I*), upper outer (*II*) and lower outer (*III*) wire mass sections

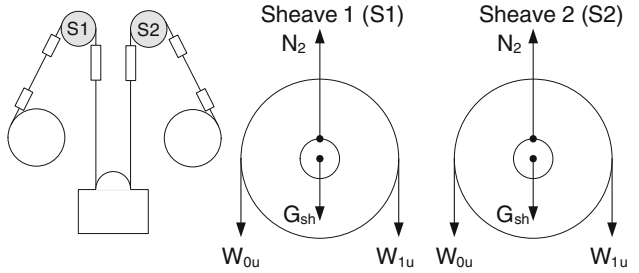


**Fig. 7** FBD's of the upper sheaves

The lower sheave (S3) moves with the combined payload giving it acceleration $\ddot{x}_c$, see Fig. 8. The equivalent equation for the FBD and KD is:

$$N_2 - G_{sh} - W_2 - W_3 = m_{sh}\ddot{x}_c \tag{23}$$

### 3.2.8 Bearing-pin friction

The coulomb friction equation for dry friction in the static case is used to model the bearing-pin friction: $F_f = \mu \times N$. This is only an approximation as the ideal case would be to model the kinetic friction. The friction between the three bearings and pins with normal forces from Eqs. 21, 22 and 23 inserted are:

$$F_{f1} = \mu \times abs(G_{sh} + W_{0u} + W_{1u}) \tag{24}$$

$$F_{f2} = \mu \times abs(-G_{sh} + W_1 + W_2 + m_{sh}\ddot{x}) \tag{25}$$

$$F_{f3} = \mu \times abs(G_{sh} + W_{2u} + W_{3u}) \tag{26}$$

where the friction factor between the bearing and pin is approximated as $\mu = 0.1$. The *abs* sign in front of the parenthesis means *absolute value*. It is used because the sign of the friction forces is to be determined by the rotational direction of the sheaves, see Eqs. 27, 28 and 29.

## 3.3 Rotary dynamic analysis

### 3.3.1 Sheaves

The torque consists of the wire force times the sheave radius, see Fig. 9. Its sign is chosen to be positive in the counter clockwise rotational direction.

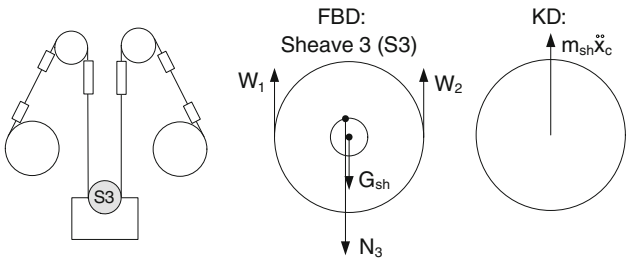


**Fig. 8** The FBD and KD of the lower sheave

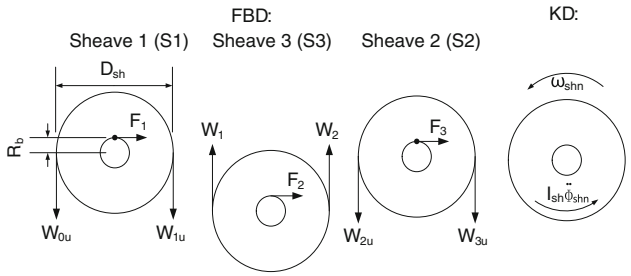


**Fig. 9** FBD's and KD for the sheaves showing rotary dynamics

Inserting the friction forces Eqs. 24, 25 and 26 in with the equivalent equations for the FBD's and KD yields:

$$\frac{D_{sh}}{2}(W_{ou} - W_{1u}) - \mathrm{sgn}(\phi_{sh})N_u \times \mu \times R_b = I_{sh}\ddot{\phi}_{sh1} \tag{27}$$

$$\frac{D_{sh}}{2}(-W_1 + W_2) - \mathrm{sgn}(\phi_{sh})N_u \times \mu \times R_b = I_{sh}\ddot{\phi}_{sh2} \tag{28}$$

$$\frac{D_{sh}}{2}(W_{ou} - W_{1u}) - \mathrm{sgn}(\phi_{sh})N_u \times \mu \times R_b = I_{sh}\ddot{\phi}_{sh3} \tag{29}$$

### 3.3.2 Sheave inertia

The sheave is considered a thick walled cylinder and therefore its inertia is calculated as such.

$$I_{sh} = 0.5 \times m_{sh} \times \left[\left(\frac{D_{sh\_i}}{2}\right)^2 + \left(\frac{D_{sh}}{2}\right)^2\right] \tag{30}$$

### 3.3.3 Active Drum

The torque and inertia of the active drum is investigated in Fig. 10.

From the FBD and KD we get the following equation:

$$-W_{0l}r_{drum} = I_{drum}\ddot{\phi}_{drum} \tag{31}$$

### 3.3.4 Active drum inertia

The active drum inertia $I_{ad}$ consists of the inertia of a thick-walled cylinder and two massive disks.

$$I_{ad} = I_1 + 2 \times I_2 \tag{32}$$

where $I_1 = 0.5 \times m_{cyl} \times \left[\left(\frac{d_D - 2 \cdot h_D}{2}\right)^2 + \left(\frac{d_D}{2}\right)^2\right]$ is the inertia of the thick cylinder and inertia of the massive disk is $I_2 = 0.5 \times m_{DE} \times \left(\frac{d_{DE}}{2}\right)^2$.

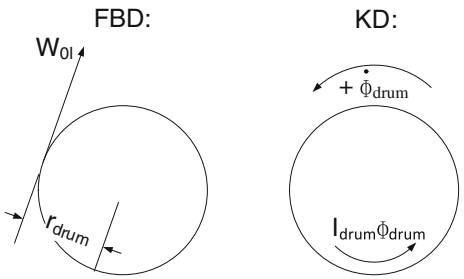


**Fig. 10** The FBD and KD for the active drum

### 3.4 Sheave-wire slippage

The maximum wire force $W_{0u\ max}$ before slippage occurs needs to be calculated to ensure no slippage will occur. This is done using *Eytelwein's formula*:

$$W_{0u\,\max} = W_{1u} \times e^{\mu_{wsh}\beta} \tag{33}$$

where the friction constant between wire and sheave is assumed to be: $\mu_{wsh} = 0.25$. The contact angle is estimated to be: $\beta = \pi$. The equation variables are depicted in Fig. 11.

This test is calculated for sheave 1 for all calculated configurations of the mechanical system, see Table 2. The results show $W_{0u\ max}$ to be over double that of the acting wire force $W_{1u}$, meaning no slippage occurs. It is assumed that if the test holds up for sheave 1, the rest of the sheaves are also safe from slippage.

## 4 Hydraulic system modeling

Using the steady state design approach as described by Stecki and Garbacik [25] a hydraulic circuit concept was proposed. This design method doesn't take into consideration the actual dynamics of the system, so the designed system must be verified during the simulation phase. The proposed hydraulic circuit consists of two hydraulic power units, two servo valves, a hydraulic motor, and a gearbox. Fig. 12 illustrates this hydraulic circuit concept.

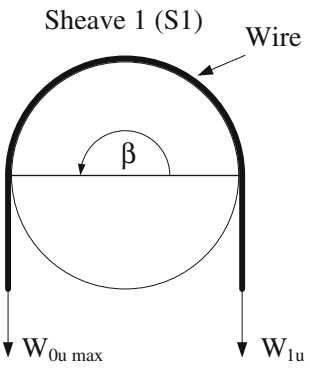


**Fig. 11** Illustrating Eytelwein's formula

### 4.1 System dimensioning

The results of the hydraulic system dimensioning are compiled in Table 2. Each subsection of Sect. 4.1 shows the method in which these dimensions were determined.

#### *4.1.1 Operating cycle*

The operating cycle defines the required motor angular velocity across an operating cycle. Starting with the platform heave velocity which is obtained by deriving Eq. 10:

$$\dot{z}(t) = 2 \times \pi \times f \times \cos(2 \times \pi \times f \times t) \tag{34}$$

and by inputting $f = 0.1$ Hz and using an amplitude of 1, this yields a total cycle time of 10 s. The maximum velocity of the platform becomes: $\dot{z}(0) = 0.628\frac{m}{s}$. The maximum active drum angular velocity (rpm) then becomes:

$$n_{drum\_\max} = \frac{30 i_{sh} \times \dot{z}(0)}{\pi r_{drum}} \tag{35}$$

which is used in dimensioning the gearbox, see the following subsection.

Relating the platform velocity to the hydraulic motor gives the following motion reference equation for the motor angular velocity:

$$\omega_{motor}(t) = \frac{i_{gear} \times i_{sh} \times \dot{z}(t)}{r_{drum}} \tag{36}$$

Finally, the required torque from the motor $\tau_m$ is calculated. First the motor acceleration is found:

$$\dot{\omega}_{motor}(t) = \frac{i_{gear} \times i_{sh} \times \ddot{z}(t)}{r_{drum}} \tag{37}$$

where the platform acceleration is the time derivative of Eq. 33: $\ddot{z}(t) = -4\pi^2 f^2 \sin(2\pi \times f \times t)$. This gives a maximum platform acceleration of $\ddot{z}(2.5) = -0.395\,m/s^2$ and $\ddot{z}(5) = 0.395\,m/s^2$. This is considered small enough to disregard. Thus, the motor torque becomes:

$$\tau_m \approx \frac{\tau_{drum}}{i_{gear}} \tag{38}$$

#### *4.1.2 Gearbox*

A gearbox size can be determined by using the required drum torque $\tau_{drum}$ (from Table 1) and choosing an equivalent or larger value for nominal torque $\tau_{2n}$ in a gearbox catalogue. The next step is to determine the output duration factor

$$f_{h,required} = n_2 \times h_r \tag{39}$$

**Table 2** Initial parameters for the hydraulic system connected to the three-sheaved mechanical system

| Component | Component quantity | Parameter | Symbol | Quantity |
|---|---|---|---|---|
| Gearbox | *1* | Reduction ratio | $i_{gear}$ | 23.2 |
| | | Life duration | $h_r$ | 500 h |
| | | Cost | $C_{GB}$ | 5.77 |
| Hydraulic motor | *1* | Displacement | D | 250 $cm^3$ |
| | | Pressure drop over motor | $p_m$ | 260 bar |
| | | Hydromechanical efficiency | $\eta_{hmM}$ | 0,92 |
| | | Cost | $C_m$ | 2.5 |
| *Servo valve* | *2* | Nominal flow | $q_{v\_nom}$ | 200 l/min |
| | | Cost | $C_{sv}$ | 10.0 |
| Hydraulic power unit (HPU) | *2* | Max. pressure provided | $p_{max}$ | 260 bar |
| | | Cost | $C_{HPU}$ | 12.0 |

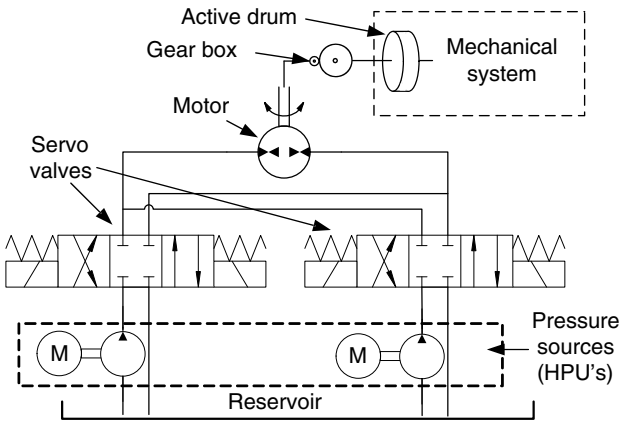


**Fig. 12** The hydraulic circuit concept

where $h_r$ is the life duration for the system, which is 500 h, and $n_2$ is the angular output speed that is equal to the maximum active drum speed as given by Eq. 35.

#### *4.1.3 Hydraulic motor*

To determine the size of the hydraulic motor $D_M$, calculation of the minimum motor discharge displacement $D_{M,min}$ is needed. When choosing a hydraulic motor from a datasheet, its displacement should be $>D_{M,min}$. The equation below is used to determine this component:

$$D_{M,min} = \left(\frac{2\pi \times \tau_M}{p_M}\right) \times \frac{1}{\eta_{hmM}} \tag{40}$$

where the required motor torque $\tau_m$ is given by Eq. 38. The hydromechanical efficiency ($\eta_{hmM}$) and motor pressure ($p_M$) depend on the type of motor chosen and can be found in datasheets for the chosen motors.

Once the duration factor has been calculated, one can use a data table for gearboxes to choose a reduction gear ratio that is suitable for the working conditions required $\tau_2 \geq \tau_{drum}$ and $f_h \geq f_{h,required}$.

#### *4.1.4 Servo valves*

The size and number of the servo valves is determined by the required motor flow, $Q_M$:

$$Q_M = \frac{D_M \times n_M}{1000\,\eta_{vm}} \tag{41}$$

where $n_M$ is the motor speed, $\eta_{vm}$is the volumetric efficiency of the motor.

#### *4.1.5 Hydraulic power units*

The pressure drop over the servo valves is 70 bar. The chosen pressure level is 150 bar. Thus, it was decided to choose an HPU with 260 bar since this gives an excess of: 260 − 150 – 70 = 40 bar which can allow for potentially bigger pressure differentials.

## 5 Control architecture

For controlling the draw-works in load case 1 and 2 a cascaded controller was used, see Fig. 13. The outer controller is a P-controller while the inner controller is a PI-controller. The main reason for using this setup is that the controller's job is two-fold: one is to heave compensate, the other is to lower the payload 5 m. Combining these two load cases could prove difficult for a single controller feedback system. Therefore, a cascaded controller is selected.

The outer controller is used for positioning the payload. Therefore, its set point is in motor angular displacement. The process variable of the outer loop is the angular displacement of the motor. The output of the outer controller is added with the inner loop set point.

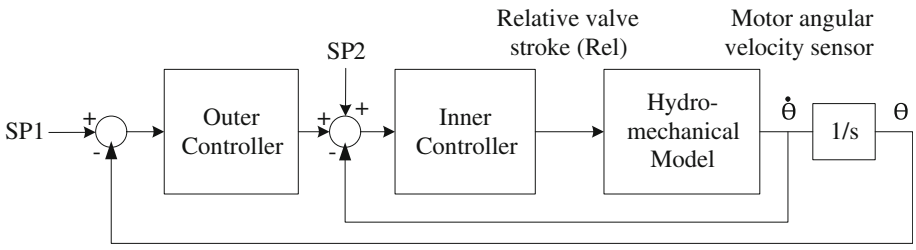


**Fig. 13** Cascade control architecture for the draw-works

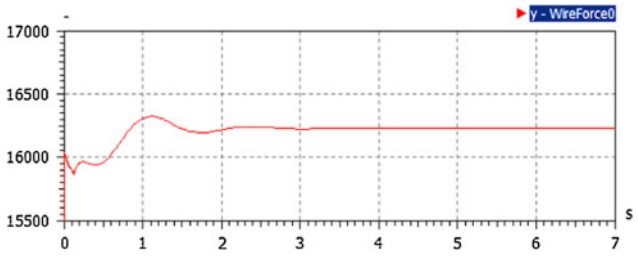


**Fig. 14** Simulation result for the wire force in steady state

## 6 Simulation

The equations of motion of the mechanical system and component dimensions of the hydraulic system are implemented in *SimulationX*. Simulation results for wire force and active drum torque were gathered, see Fig. 2. The authors ran several sets of simulations for sheave configurations up to 13 sheaves with increments of 2. The simulation results are summarized in Table 2.

### 6.1 Verification of dimensions

The reason for gathering these results is because the dimensioning of the hydro-mechanical system starts with the values of the wire force and active drum torque. The values for the simulated results are taken as the system has reached equilibrium at and beyond 2 s in Fig. 13 and 14. The reason for the transient response between 0 to 2 s is because of a slight slack in the wire present in the model.

The simulation results are compared with the statically calculated parameters, see Table 3. The results show that all statically calculated wire forces are lower than the simulated ones. Since the wire force is a significant part of dimensioning the mechanical system, it means most of the mechanical system is under dimensioned. The opposite is true for the statically calculated active drum torques, which means the hydraulic system has been over dimensioned. By adjusting the design parameters to close the gap between calculated and simulated values of wire force and active drum torque more optimized designs are achieved. The simulated values in Table 2 also represent the final design limits for the hydro-mechanical systems.

### 6.2 Cost analysis

Cost analysis using a dimensionless unit was conducted for both mechanical and hydraulic systems. By combining these two, a total hydro-mechanical cost analysis was achieved. Table 4 indicates that the hydro-mechanical system with seven sheaves is the most cost efficient. This system will therefore be used.

### 6.3 Load case 1 and 2

Both load case 1 and 2 have been simulated for the hydro-mechanical system with 7 sheaves to verify the model. The results indicate that the design is within designed limits and operates satisfactorily. Figs. 15, 16 show the payload displacement results for load case 1 and 2. It can be observed that the model stabilizes and lowers the payload gently to the desired position. A zoomed in image of load case two shows the payload position as it hits the seabed, see Fig. 17.

The average wire force and active drum torque occurring during load case 2 are within the design limits, see Fig. 18 and 19. This means the system is also within limits for load case 1 because vertical position stabilization of the payload continues after the payload has been lowered. This

**Table 3** Comparison of static calculations and simulated results

| Datum | Symbol | 3 Sheaves | 5 Sheaves | 7 Sheaves | 9 Sheaves | 11 Sheaves | 13 Sheaves |
|---|---|---|---|---|---|---|---|
| Wire force | N | 40,940 | 20,960 | 14,300 | 10,970 | 8,970 | 7,640 |
| Simulated wire force | N | 45,680 | 23,480 | 15,965 | 12,165 | 9,956 | 8,624 |
| Slippage wire force | N | 89,793 | 45,971 | 31,364 | 24,060 | 19,674 | 16,757 |
| Active drum torque | Nm | 12,880 | 5,140 | 2,660 | 1,730 | 1,280 | 1,100 |
| Simulated active drum torque | Nm | 10,860 | 4,395 | 2,473 | 1,592 | 1,217 | 939 |

**Table 4** Cost analysis for different hydro-mechanical system configurations

| System cost | 3 sheaves | 5 sheaves | 7 sheaves | 9 sheaves | 11 sheaves | 13 sheaves |
|---|---|---|---|---|---|---|
| Mechanical | 4.52 | 4.49 | 4.72 | 5.05 | 5.44 | 5.73 |
| Hydraulic | 30.27 | 28.86 | 27.52 | 27.42 | 27.07 | 27.07 |
| Total cost coefficient | 34.79 | 33.35 | 32.24 | 32.47 | 32.51 | 32.8 |

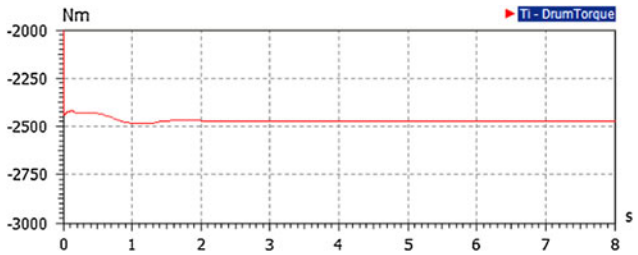


**Fig. 15** Simulation result for the active drum torque in steady state

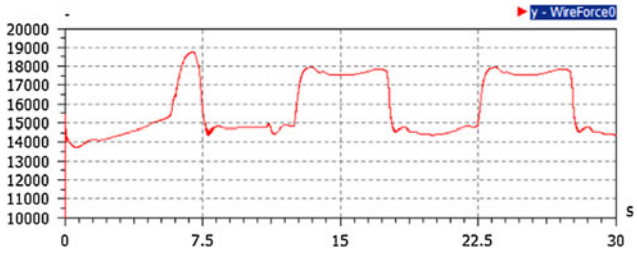


**Fig. 19** Simulated wire force during load case 2

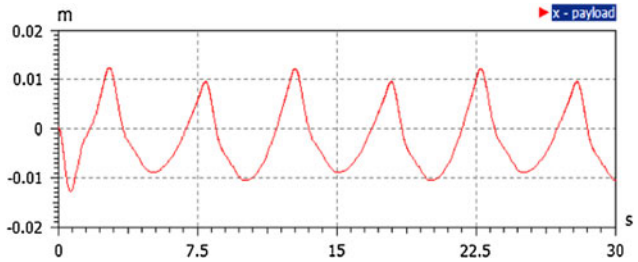


**Fig. 16** Simulation result for load case 1 with AHC system on showing ca. ±1 cm in position oscillation

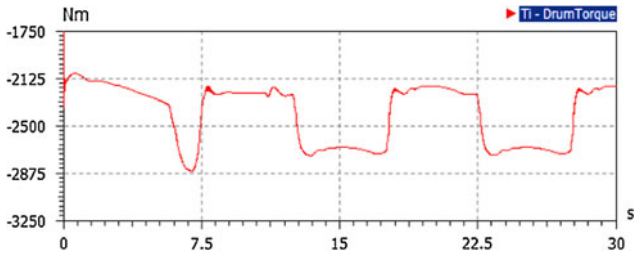


**Fig. 20** Simulated active drum torque during load case 2

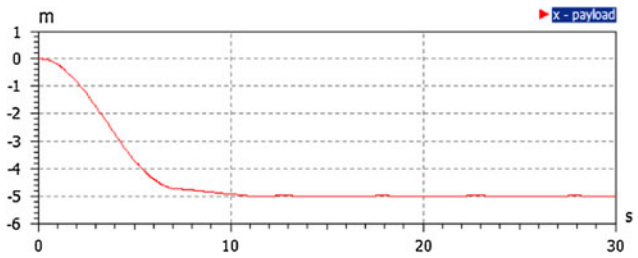


**Fig. 17** Simulation result for payload lowering of 5 m onto the seabed—load case 2

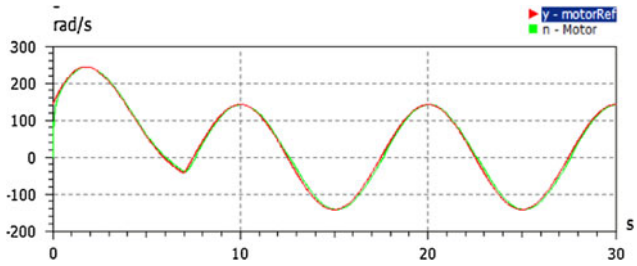


**Fig. 21** Motor reference angular velocity (motorRef) and actual velocity (Motor) curves during load case 2

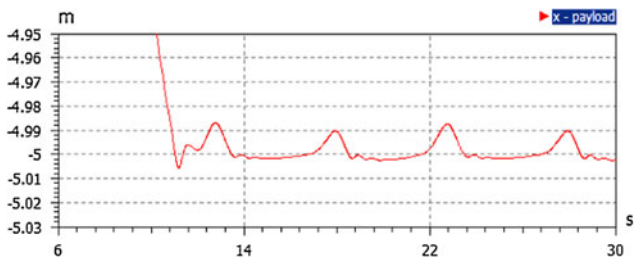


**Fig. 18** A zoomed in view of payload position during load case 2

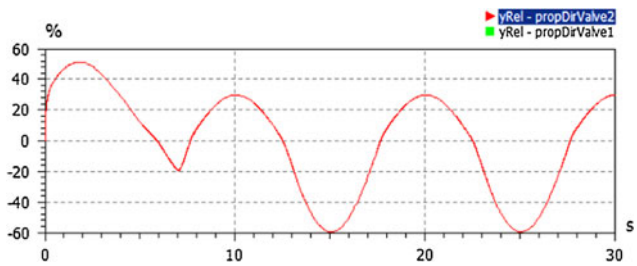


**Fig. 22** Curves for relative valve stroke for the two servo valves during load case 2

is shown by Fig. 20 where the motor angular velocity reference curve overlaps the actual angular velocity. The relative valve stroke of both servo valves show they are operating well within their limits of 100%, see Fig. 21.

## 7 Conclusion

A simulation model of an active heave compensation system was developed for a draw-works on a hoisting rig. Important components and dynamics of the draw-works and hoisting rig were dimensioned, modeled and set up in simulation software *SimulationX*. A cost optimization process was completed yielding the final configuration of 7 sheaves in total. A control architecture was set up where the controller regulates a pair of servo valves. The feedback signals were the motor angular displacement and velocity. The chosen controller algorithm was a cascaded P-PI controller which was also implemented in the simulation model. Simulations run for load case 1 and 2 showed that the hydro-mechanical system parameters are within their design limits.

This work sets the foundation for future work which includes a hardware-in-the-loop test in which a physical controller is tested and tuned with the mathematical model presented in this paper.

**Acknowledgment** The authors would like to direct a special thanks to Professor Geir Hovland for his kind assistance in providing us with the needed Hardware, literature and the operation instruction. Further thanks to the technical staff at the Mechatronics laboratory of the University of Agder for the dedication and the enthusiasm which helped and motivate us to reach the project goals.

## Appendix A. *SimulationX* model

Mechanical model implementation

This section shows how the simulation model was implemented from the equations of motion for the mechanical system. The system was set up from the payload and upwards toward the active drum. The structure of each major part: combined payload, wire dynamics, sheave system, bearing-pin friction are explained briefly. The actual values and references used in the simulation blocks are included in the sections below.

### A.1 Combined payload

*External forces*

The payload is modeled by a *mass* component. It is attached to by five external forces. These are the forces described in Eq. 1. For clarification, *Pulling Force* in the simulation model consists of the wire forces pulling the payload. *PayloadIni* gives the initial position of the payload so that it starts in a position where the wires are very close to outstretched to reduce initial oscillations. It is derived in this way:

$$x_{ini} = \frac{F}{n \times k}$$

where $n$ is the number of wires connected to the combined payload. The other blocks are self-explainable.

*Inertia*

The *Mass* block automatically calculates the linear inertia from the parameters put into it, thus not requiring any additional input from the user.

*Seabed dynamics*

Seabed dynamics is implemented by adding the damping force component with the spring force component and feeding the result into the *SeabedDynamics* function. The important thing about the seabed dynamics is that it must only activate if the payload position is at $-5$ m. An if-else statement is made in *Damping* and *Stiffness* to account for this.

### A.2 Wire dynamics

The *Wire dynamics* part includes the equations for wire forces (Eqs. 2, 3, 4 and 5), elongation (Eqs. 6, 7, 8 and 9) and rate (Eqs. 11, 12, 13 and 14. Additionally, there are *function* blocks with data of outer and inner wire section masses: *halfwmass*0 and *halfwmass*1 respectively.

To aid calculation of the total lower wire mass *Nr* is multiplied with *PerMeter* and *halfwmass*1. The *Nr* block is for the number of wire sections and *PerMeter* is for the mass per meter datum derived from the *mass per* 100 *m* from the *Certex* wire catalogue. This datum is included in the *payload* block in the *CombinedPayload* part.

*Wire force*

The wire forces are implemented in the *WireForce* block. The spring stiffness and damper coefficients are fed into these blocks through the *WireStiffness* and *WireDamping* blocks. The wire cross-sectional area is written in block *SpringArea* and used in finding the wire stiffness.

The inner wire forces (*WireForce1, WireForce2*) calculated in this part is used in the *PullingForce* block in part

*Combined Payload*. Both inner and outer wire forces are used in calculating sheave and drum torques (*SheaveTorque* and *Active* blocks) and normal force in bearing-pin friction (*Normal* blocks).

*Elongation and rate*

Equations for wire elongation and rate are put in the *Elongation* and *Rate* blocks. Their outputs are sent to the *WireForce* blocks.

*Wire mass and inertia*

The blocks *halfwmass*0 and *halfwmass*1 depict half the outer and inner wire section masses respectively. They are used in

- the blocks *DrumTorque*, *sheavetorque* 1 and 2 to account for the wire mass' effect on the drum and outer sheave torques.
- The normal forces in the bearing-pin friction part (*Normal* blocks).
- the *payload* block as part of the combined payload, thereby having the lower wire section mass' inertia modeled. Its effect on the elongation will also be included by doing this.

## A.3 Sheave system

This part contains the sheaves, active and passive drums and a subpart called *Component Dimensions* which have *Function* blocks containing data for the component dimensions.

*Sheave mass and inertia*

The travelling block sheave's mass is included in the *payload* block in the *Combined Payload* part. This accounts for the linear inertia of the sheave. The crown block sheaves have no linear inertia in relation to the power source so they are not included. The sheave's rotational inertia is implemented through the *Inertia* block. This value is calculated from Eq. 30.

*Sheave torque*

The sheaves' torques are modeled by attaching *External Torque* blocks to the *inertia* blocks with equations from Eqs. 27, 28 and 29.

*Active drum*

The active drum is set up in the same fashion as the sheaves with *Inertia* blocks representing the inertia calculated in Eq. 32. The active drum torque is also modeled by attaching an *External Torque* block to its *inertia* block. The *External Torque* block had to be connected from the right side of the *Inertia* block because of the need of a *Preset* block. Doing this makes the torque act against the coordinate direction, thus the value inside this block needs to have a minus sign to reverse this effect. The *preset* allows the user to set a prescribed state of motion. For example, to hold the drum still a *fixed* state can be set. This function will prove useful in verifying the static analysis results. When the mechanical model is attached to the hydraulic model later on this preset is removed and attached to the gearing.

*Component dimensions*

In this subpart the radius for the active drum, sheaves and sheave bearings are stored in *function* blocks. The inertia of the active drum and sheave are also stored in *function* blocks along with the sheave mass. The outputs of these blocks are subsequently referred to the *inertia* and *External Torque* blocks for the active drum and sheaves. The *SheaveMass* is used in the *bearing-pin* part.

## A.4 Bearing-pin friction

The *Bearing-Pin Friction* part of the simulation model contains functions of the normal forces that are used to calculate the bearing-pin frictions. The Eqs. 21, 22 and 23 are implemented in these blocks. The data in the *Normal* blocks are referred to the *sheavetorque* blocks where they are multiplied with the bearing radius and bearing-pin friction coefficient to include the effects of friction on the sheaves' torques. The data in the *Normal* blocks are absolute values.

*Function 1, 2, 3*

These *Function blocks* include if-else statements that create a transitional slope $<1$ for when the friction moment changes direction. Before implementing this feature, *SimulationX* would have issues simulating the system due to the sharp directional changes of the sheaves.

*Heave motion*

This part has one *signal block* generating a sine wave with the parameters of the heave motion as per Eq. 10. Its output is included in the *Elongation* blocks to account for the heave motion's effect on wire elongation Fig. 22.

*Hydraulic model*

Implementation of the hydraulic model follows the same method as that of the mechanical one. The relevant

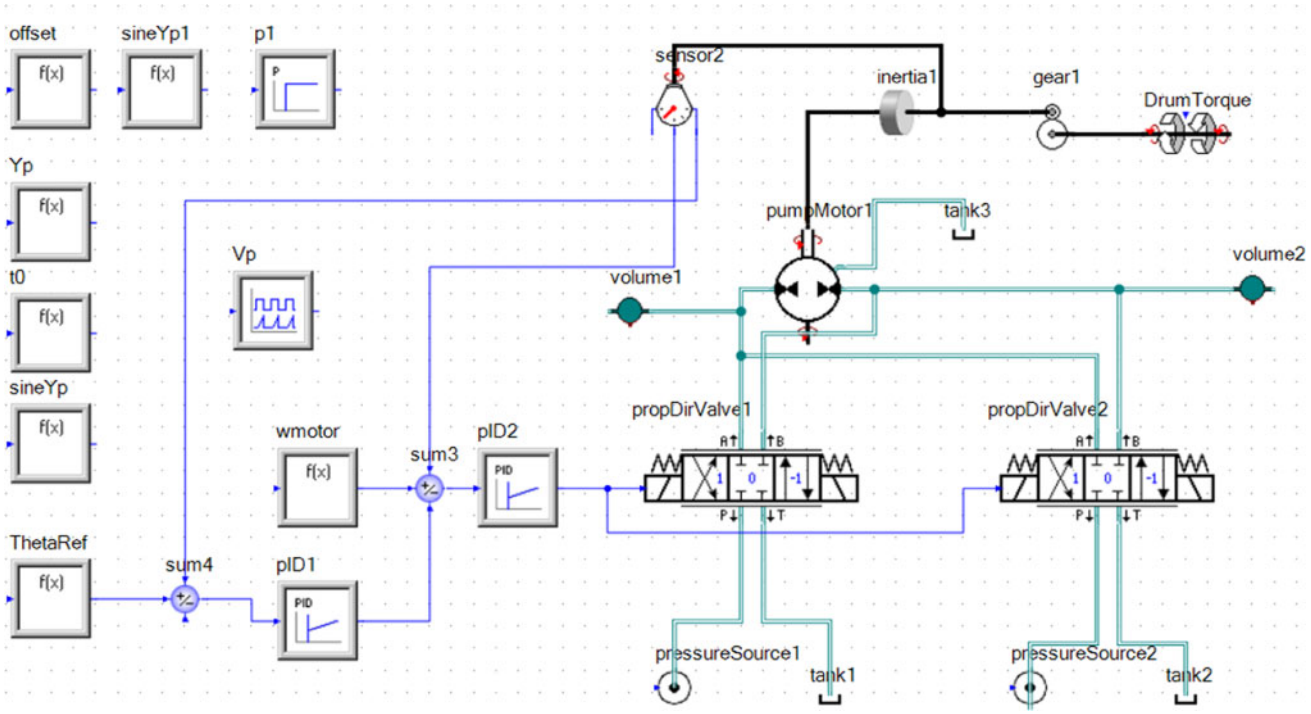


**Fig. 23** *SimulationX* model of the hydraulic system with three sheaves

simulation components with the correct dimensions are used. The result is the model seen in Fig. 23.

*Model fusion*

Putting the mechanical and hydraulic models together is achieved by connecting the gear component to the active drum component.

## References


1. Haltleskog JT, Dunnigan MW (2006) Heave compensation simulation for non-contact operation in deep water. Oceans 2006:1–6
2. Korde UA (1998) Active heave compensation on drill-ships in deep water. Ocean Eng 25(7):541–561
3. Sagatun SI, Johansen TA, Fossen TI, Nielsen FG (2002) Wave synchronizing crane control during water entry in offshore moonpool operations. In: Proceedings of the IEEE Conference on Control Applications, Glasgow, Scotland, UK, pp 174–179
4. Skaare B, Egeland O (2006) Parallel force/position crane control in marine operations. IEEE J Ocean Eng 31(3):599–613
5. Messineo S, Celani F, Egeland O (2007) Crane feedback control in offshore moonpool operations. Control Eng Pract. doi: 10.1016/j.conengprac.2007.05.003
6. Sagatun SI (2002) Active control of underwater installation. IEEE Trans Control Syst Technol 10(5):743–748
7. Godhavn JM (1998) Adaptive tuning of heave filter in motion sensor. Proc Ocean 1(1998):174–178
8. Haltleskog JT, Dunnigan MW (2006) Passive compensator load variation for deep water contact operations. Oceans 2006:1–6
9. Driscoll FR, Buckham B, Nahon M (2000) Numerical Optimization of a Cage-Mounted Passive Heave Compensation System. Oceans MTS IEEE Conf Exh J 2(4):1121–1127
10. Ni J, Liu S, Wang M, Hu X, Dai Y (2009) The simulation and research on passive heave compensation system for deep sea mining. In: Proceedings of IEEE international Conference on Mechatronics and Automation, pp 5111–5116
11. Ocean Drilling Program (2010) Active Heave Compensator (Online). Available at: http://www-odp.tamu.edu/publications/tnotes/tn31/pdf/ahc.pdf
12. Neupert J, Mahl T, Haessig B, Sawodny O, Schneider K (2008) A heave compensation approach for offshore cranes. In: American Control Conference 2008, pp 538–543
13. Li L, Liu S (2009) modeling and simulation of active-controlled heave compensation system of deep-sea mining based on dynamic vibration absorber. In: Proceedings of IEEE international conference on Mechatronics and Automation, pp 1337–1341
14. Xiao J-Z, Wang H-R, Yang X-C, Gao Z (2011) Multiple faults diagnosis in motion system based on SVM. Int J Mach Learn Cybern. doi: 10.1007/s13042-011-0035-y
15. Zheng H, Liu S, Yang N (2011) Hardware-in-the-loop Simulation System and Its Visual Monitoring of Heave Compensation. In: Proceedings of the ninth ISOPE ocean mining symposium, pp 131–137
16. Shah NH, Shukla Kunal T (2010) Optimal production schedule in declining market for an imperfect production system. Int J Mach Learn Cybern 1(1–4):89–99
17. Lin C-M, Li M-C, Ting A-B, Lin M-H (2011) A robust self-learning PID control system design for nonlinear systems using a particle swarm optimization algorithm. Int J Mach Learn Cybern 2(4):225–234
18. Zhang X, Liu S, Zeng F, Li L (2010) Simulation Research on the Semi-active Heave Compensation System Based on $H\infty$ Robust Control. In: Proceedings of international conference on intelligent system design and engineering application, pp 378–382

19. Certex (2011) Product catalogue: blocks and sheaves (Online). Available: http://www.certex.com/products/13.pdf
20. Jensen GA, Safstrom N, Nguyen TD, Fossen TI (2010) A nonlinear PDE formulation for offshore vessel pipeline installation. Ocean Eng 37:365–377
21. Fathi D (2004) ShipX Vessel Responses (VERES). MARINTEK, Trondheim http://www.marintek.sintef.no
22. WAMIT (2004) WAMIT User Manual http://www.wamit.com
23. Fossen TI (2002) Marine control systems: guidance, navigation, and control of ships, rigs and underwater vehicles, 1st edn. Marine Cybernetics, Trondheim
24. Fossen TI, Smogeli ØN (2004) Nonlinear time-domain strip theory formulation for low-speed maneuvering and station-keeping. Model Identif Control 25(4):201–221
25. Stecki JS, Garbacik A (2002) Design and steady-state analysis of hydraulic control systems. Fluid Power Net Publications, Cracow